

Spin-mechanics with color centers in hexagonal boron nitride membranes

Mehdi Abdi, Myung-Joong Hwang, Mortaza Aghtar, and Martin B. Plenio

Institut für Theoretische Physik und IQST, Albert-Einstein-Allee 11, Universität Ulm, 89069 Ulm, Germany

(Dated: April 4, 2017)

Recently observed quantum emitters in hexagonal boron nitride (hBN) membranes have a potential for achieving high accessibility and controllability thanks to the lower spatial dimension. Moreover, these objects naturally have a high sensitivity to vibrations of the hosting membrane due to its low mass density and high elasticity modulus. Here, we propose and analyze a spin-mechanical system based on color centers in a suspended hBN mechanical resonator. Through group theoretical analyses and *ab initio* calculation of the electronic and spin properties of such a system, we identify a spin doublet ground state and demonstrate that a spin-motion interaction can be engineered which enables ground state cooling of the mechanical resonator. We also present a toolbox for initialization, rotation, and readout of the defect spin qubit. As a result the proposed setup presents the possibility for studying a wide range of physics. To illustrate its assets, we show that a fast and noise resilient preparation of a multicomponent cat state and a squeezed state of the mechanical resonator is possible; the latter is achieved by realizing the extremely detuned, ultrastrong coupling regime of the Rabi model, where a phonon superradiant phase transition is expected to occur.

Introduction.—Recently, there have been an increasing number of reports on the observation of optical single photon emitters in mono- and multi-layer hexagonal boron nitride (hBN) samples in room and cryogenic temperature setups [1–3]. The single-photons emitted from hBN have very narrow and pronounced zero-phonon-line [2]. Additionally, the emitters have the privilege of being hosted in a 2D material, giving them the advantage of a high accessibility and sensitivity [4]. The hexagonal boron nitride membranes have low mass yet high elasticity modulus and tensile strength, which make them promising candidates for high quality mechanical resonators [5–7]. Their extremely small out-of-plane stiffness also gives them a large zero-point amplitude, i.e. a high motion sensitivity. The origin of hBN emitters has yet to be explored and despite the *ab initio* computational work in Ref. [1], which attributes the emissions to charge neutral *anti-site complex* defects $V_N N_B$ [Fig. 1a], a group theory support is still missing.

In this Letter, we perform group theory analyses and *ab initio* computations to study the electronic structure and spin properties of $V_N N_B$ defects. Based on this knowledge we propose, for the first time, a setup for coupling a spin state of the color centers hosted in a suspended hBN flake to its vibrational modes [6, 8]. Taking advantage of the exceptional geometry of the proposed setup, a manipulation toolbox for the spin qubit—and through it the mechanical mode—is proposed here. This includes initialization, rotations, and readout of the spin qubit via optical excitations and microwave drives. By employing collimated light beams and tunable microwave drives each spin qubit can be individually addressed. Regarding the mechanical mode, we shall first demonstrate the possibility of cooling a vibrational mode of the membrane (with frequency ω_m) down to its ground state by the resolved sideband technique. We also show that the spin-motion coupling rate g_0 can reach and even exceed the

fundamental mechanical mode frequency $g_0 \gtrsim \omega_m$, realizing the so-called ultrastrong coupling regime [9–12]. Based on such a large coupling rate, we explore the possibility of the fast preparation of nonclassical states of a mechanical mode of the membrane and demonstrate that both multicomponent Schrödinger cat states [13, 14] and highly squeezed states can be prepared within less than a mechanical period. While the former makes use of the spin-dependent displacement of the motion, the latter is achieved by effectively realizing the Rabi model in the extremely detuned, ultrastrong coupling regime. The possibility to realize this regime of the Rabi model opens a door to study the recently predicted superradiant phase transition [15, 16] in this setup providing an alternative to earlier ion trap setups, which rely on interaction picture [17]. The ability to prepare the hBN flake in these nonclassical states can also open an avenue for exploring the macroscopic quantum physics.

Model.—We consider the $V_N N_B$ defect of a monolayer hBN membrane, depicted in Fig. 1a. As group theory analyses predict, consistent with *ab initio* computations, the ground and excited electronic states—which constitute our manifold of interest—are spin doublets; the results are summarized in Fig. 1b and c (See the supplemental material for more details and a rigorous treatment [18]). Due to dipole allowed transitions, the excited states spontaneously decay to the ground state at the rate κ while preserving the spin projection. Meanwhile, a spin-orbit interaction mixes spin states of the two manifolds, inducing spin-flip transitions (the straight lines in Fig. 1c). Spontaneously, such transitions are dominated by the spin preserving ones. However, they can be driven by a collimated optical beam with a proper in-plane polarization. When the setup is immersed into a magnetic field, the spin degeneracies are lifted. We exploit these two properties and propose an optical mechanism for initializing the spin state of the ground man-

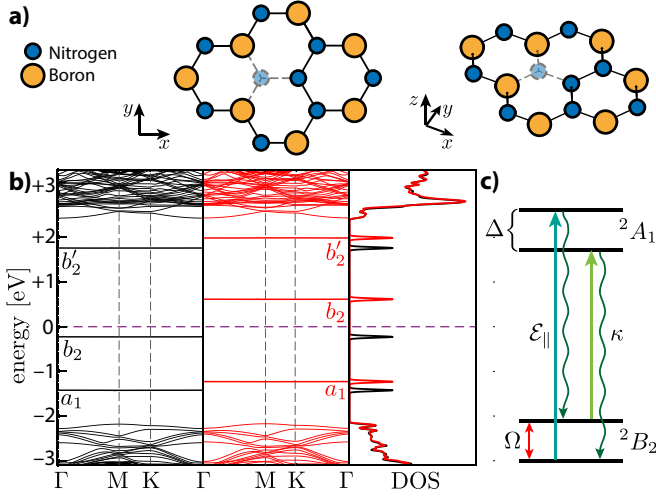


FIG. 1. a) Geometry of $V_N N_B$ defect in hBN monolayer in top (left panel) and tilted (right panel) views. b) *ab initio* results for band structure and the corresponding density of states (DOS) of a monolayer hBN with charge neutral $V_N N_B$ defects: Spin-up polarization is in black and spin-down in red. The defect energy levels within the band-gap are labeled according to their molecular symmetry [18]. The Fermi energy level is set to zero (purple dashed line). c) Two lowest multi-electron states of the defect. They are spin doublets with Zeeman splitting Δ and the respective transition rates: spin-preserving decays (at rate κ), spin-flip optical drives due to spin-orbit mixing $\mathcal{E}_{||}$, and microwave drive Ω .

ifold [18]. The induced spin relaxation rate Γ is only bounded from above by $\Gamma \leq \kappa$. Hence, it can in principle be switched off—when there is no optical drive, $\mathcal{E}_{||} = 0$. This spin-dependent resonant excitation mechanism also allows single-shot projective readout of the spin [19, 20].

The hBN single-photon emitters have shown intrinsic electronic sensitivity to the local strain [2]. However, the observed deformation potential [21] results in very weak zero-point-motion coupling rates (compared to the excited state lifetime) and thus electronic and motional dynamics cannot appreciably influence each other. Instead, since the ground state of $V_N N_B$ color centers is a spin doublet, their electronic spin degree of freedom can couple to the motion of the membrane via field gradient of a magnetic tip [22–26] (see Fig. 2a for the proposed setup). The spin-motion coupling rate also depends on the geometry of the membrane and the location of the defect. Hence, it gives the opportunity of investigating various physical phenomena in different working regimes, simply by addressing individual color centers located at different sites.

High quality factors for hBN flake mechanical resonators allow us to single out a mechanical mode. Moreover, assuming weak optical drives ($\mathcal{E}_{||} \ll \kappa$), the dynamics of the excited states can be adiabatically eliminated and the $V_N N_B$ system is described by an effective two-level system, the electronic ground state spin qubit [27].

One thus deals with qubits coupled to an isolated mechanical harmonic mode, yet driven and manipulated by classical electromagnetic waves. The following Hamiltonian describes coherent evolution of our system with N spin qubits

$$\hat{H}_N = \omega_m \hat{b}^\dagger \hat{b} + \sum_{j=0}^{N-1} \frac{\Omega_j}{2} \hat{\sigma}_{x,j} - \frac{\delta_j}{2} \hat{\sigma}_{z,j} + g_j \hat{\sigma}_{z,j} (\hat{b} + \hat{b}^\dagger), \quad (1)$$

where, $\delta_j = \omega_D - \Delta_j$ is the detuning of the microwave drive frequency from the qubit splitting and Ω_j is the Rabi frequency. Here, \hat{b} (\hat{b}^\dagger) refer to the phonon annihilation (creation) operators of the mechanical mode and $\hat{\sigma}_x$ and $\hat{\sigma}_z$ are the Pauli matrices. The magnetic tip underneath the membrane provides a radially symmetric non-uniform magnetic field, which results in a position-dependent splitting and a spin-motion coupling for each spin qubit. The splitting $\Delta_j \equiv \Delta(r_j, \theta_j) = \mu_B g_e B_\perp(r_j, \theta_j, z=0)$, with μ_B the Bohr magneton and g_e the electron g-factor, is determined by a sum of the local magnetic field of the tip and an external uniform bias. The non-uniformity of the magnetic field on the other hand provides the spin-motion coupling, which, in the leading order, is linearly proportional to the mechanical position. The coupling rates are given by $g_j \equiv g(r_j, \theta_j) = \mu_B g_e \partial_z B_\perp(r_j, \theta_j, 0) z_{o,j}$, where $z_{o,j} = \psi(r_j, \theta_j) \sqrt{\hbar/2m\omega_m}$ is the amplitude of the membrane zero-point-fluctuations at location of the defect with mode profile function ψ and the effective mass m of the mechanical mode. In Hamiltonian (1) we have neglected the spin dipole interactions between qubits. This is indeed the case when the defects are separated by a few hundreds of unit cells.

Fig. 2b and c present the coupling rates achievable in our system. Here, the fundamental vibrational mode of a circularly clamped monolayer hBN membrane with radius R with a dominant built-in tensile strain is taken as the mechanical mode [14, 18]. The magnetic tip is modeled by a uniformly magnetized sphere of radius 50 nm and magnetization $\mu_0 M = 2.6$ T, where μ_0 is the vacuum permeability. The tip is considered to be positioned 20 nm below the center of membrane [23, 26], resulting in a maximum field gradient of $|\partial_z B_\perp(0, 0, 0)| \approx 270$ G/nm. Remarkably, the spin-motion coupling rate $g_0 \equiv g(0, 0)$ can become comparable or even larger than the oscillator frequency ω_m , hence the so-called ultrastrong coupling regime can be achieved [Fig. 3b]. This opens an exciting opportunity to explore the physics of ultrastrong spin-motion coupling with the ground-state cooled mechanical oscillator, as we demonstrate below. Throughout the paper, we will consider only two qubits: one in the center is used for the ultrastrong spin-motion coupling and one offset by r_c for the cooling, as depicted in Fig. 2a. The situation can be generalized easily to larger numbers of qubits. In particular, one can exploit the mechanical mode as a bus for coupling distant spin states to each

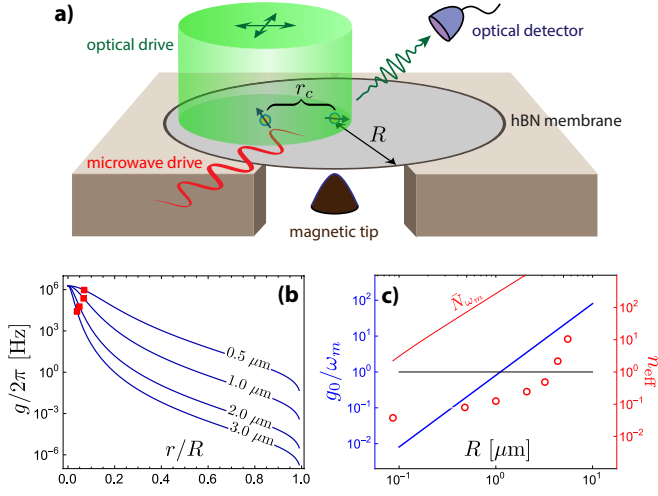


FIG. 2. a) Scheme for the proposed setup: A suspended circular hBN membrane with radius R as the mechanical resonator. A magnetic tip beneath the membrane constructs a spin-motion coupling. The spin qubits are driven by a microwave field, while a polarized collimated optical drive provides the spin polarization mechanism. b) Spin-motion coupling rate as a function of distance from the center of membrane r for different membrane radii R . The small red square on each curve denotes optimum g_c (see the text for details). c) Coupling rate to mechanical frequency ratio for the ‘central qubit’ (blue line) and effective boson number of the mechanical mode after cooling under optimal conditions (red circles) versus radius of the membrane. The black horizontal line indicates both $g_0/\omega_m = 1$ and $\bar{n}_{\text{eff}} = 1$ (the ground state limit).

other, realizing complex spin systems for quantum simulation purposes.

Cooling.—Now we study the possibility of cooling a mechanical mode of a hBN membrane by a $V_{\text{N}}N_{\text{B}}$ color center. The ground state cooling of a mechanical mode coupled to a two-level-system can be achieved for a weak coupling strength and in resolved sideband regime $\Gamma < \omega_m$ [28–30]. In our configuration the latter can be satisfied thanks to the tunability of the depolarization rate Γ . Nevertheless, one also requires a qubit weakly coupled to the resonator in order to cool the resonator to its ground state. This requirement can be fulfilled by employing a second emitter offset from the center of the membrane, where both the magnetic field gradient and amplitude of the fundamental mode vibrations are weaker. The offset r_c should be such that the coupling rate $g_c \equiv g(r_c, 0)$ satisfies $g_c < \Gamma$ yet $g_c^2 \gg \Gamma\gamma_m\bar{N}_{\omega_m}$. We call such a color center the ‘cooling qubit’. Then a microwave drive with detuning $\delta_c \approx -\omega_m$ and optimized Rabi frequency Ω can cool the resonator down to its ground state [Fig. 2c].

The full dynamics of the system is governed by the quantum optical master equation $\dot{\rho} = \mathcal{L}[\rho]$. The Liouvillian \mathcal{L} includes both coherent and irreversible dynamics of the system. In the weak coupling limit ($g_c \ll \omega_m, \Omega$)

the Liouvillian is given by

$$\mathcal{L}[\rho] = -i[\hat{H}_1, \rho] + \frac{\gamma_m}{2}((\bar{N}_{\omega_m} + 1)\mathcal{D}_{\hat{b}}[\rho] + \bar{N}_{\omega_m}\mathcal{D}_{\hat{b}^\dagger}[\rho]) + \frac{\Gamma}{2}((\bar{N}_{\Delta_c} + 1)\mathcal{D}_{\hat{\sigma}_-}[\rho] + \bar{N}_{\Delta_c}\mathcal{D}_{\hat{\sigma}_+}[\rho]) + \frac{\tilde{\Gamma}}{2}\mathcal{D}_{\hat{\sigma}_z}[\rho], \quad (2)$$

where $\gamma_m = \omega_m/Q$ is the mechanical damping rate (Q , the mechanical quality factor). Γ and $\tilde{\Gamma}$ are the qubit relaxation and decoherence rate, respectively. The bosonic thermal occupation number at temperature T is $\bar{N}_\omega = (\exp\{\hbar\omega/k_{\text{B}}T\} - 1)^{-1}$ and the Lindblad damping superoperators are $\mathcal{D}_{\hat{o}}[\rho] = 2\hat{o}\rho\hat{o}^\dagger - \hat{o}^\dagger\hat{o}\rho - \rho\hat{o}^\dagger\hat{o}$. Two main sources of qubit decoherence are considered in our analyses $\tilde{\Gamma} = \tilde{\Gamma}_o + \tilde{\Gamma}_v$ (see the last section for a discussion); dephasing induced by the optical polarization $\tilde{\Gamma}_o$ (which is comparable to the relaxation rate $\tilde{\Gamma}_o \approx \Gamma$) and the one stemming from membrane vibrations $\tilde{\Gamma}_v$. We numerically solve the steady state of the master equation ρ_{ss} with parameters: $Q = 5 \times 10^5$, $T = 30$ mK, $\Gamma = \Gamma_o = \tilde{\Gamma}_v = 0.1\omega_m$, and other parameters are optimized for the best cooling. The mean mechanical phonon numbers $\bar{n}_{\text{eff}} = \text{Tr}\{\hat{b}^\dagger\hat{b}\rho_{\text{ss}}\}$ for several R values are plotted in Fig. 2c. Remarkably, the mechanical mode can be cooled down to the ground state even for cases with large $\bar{N}_{\omega_m} \gg 1$ (see the thin red line in Fig. 2c).

Multicomponent cat state.—Here, we first note that even in the presence of a central qubit, which realizes the ultrastrong coupling with the mechanical mode, the ground state cooling can still be achieved using the cooling qubit. Owing to the r dependence of splitting $\Delta(r)$, the central qubit is off-resonant with respect to the microwave field employed for cooling $\Delta_0 \gg \Omega$; consequently, it does not significantly alter the cooling dynamics of the system [18]. Therefore, it is possible to cool down the mechanical mode to its ground state, and then to employ the central qubit for an ultrafast preparation of nonclassical states of the membrane. As an example, we put forth a protocol to prepare a multicomponent cat state of the mechanical mode, which we pursue due to its beneficial properties for continuous variable processing and metrology [31, 32]. The protocol is following: i) Once the mechanical mode is cooled down to its ground state, the spin qubit is initialized in $|\downarrow\rangle$ by the optical polarization, followed by a microwave $\pi/2$ -pulse to create a spin superposition. ii) After a quarter mechanical period, during which the spin-dependent displacement occurs, another $\pi/2$ -pulse is applied. iii) After another quarter mechanical period, a $\pi/2$ -pulse is applied, followed by the optical readout of the qubit state. The postselected mechanical state is $\frac{1}{2}[e^{2i\xi^2}(e^{-i\phi}|2\xi\rangle \pm e^{i\phi}|-2\xi\rangle) - e^{-2i\xi^2}(|-2i\xi\rangle \mp |2i\xi\rangle)]$. Here, the upper (lower) sign corresponds to the measurement outcome of spin up (down), $\xi = g_0/\omega_m$ is the spin-dependent displacement, and $\phi = \pi\Delta_0/2\omega_m$ is the accumulated phase during the first half of a mechanical

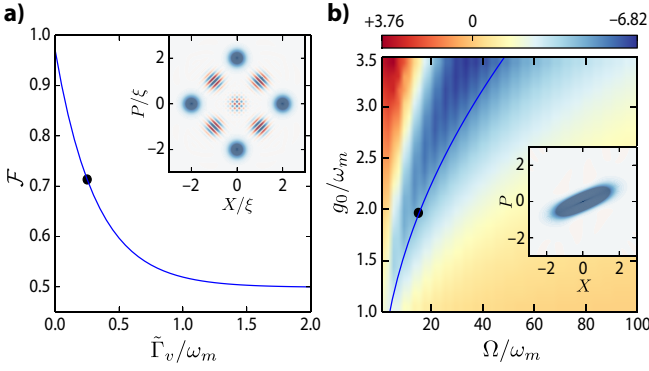


FIG. 3. a) The fidelity of the prepared multicomponent Schrödinger cat state as a function of decoherence rate. Inset: The Wigner function of the prepared state for $\tilde{\Gamma}_v/\omega_m = 0.25$ (black dot). b) The minimum quadrature variance of the mechanical mode in units of dB. Inset: The Wigner function of the prepared state for $\xi = 2$ and $\Omega/\omega_m = 15$ (black dot). In both plots $\tilde{\Gamma}_o \simeq 0$ because there is no optical polarization.

period. The fidelity of the prepared state following the above protocol for a membrane of radius $R = 1.5 \mu\text{m}$, which leads to a spin-dependent displacement of $\xi \approx 2$, is presented in Fig. 3a as a function of the vibrational decoherence rate. Thanks to the ultrafast preparation in less than a mechanical period, the prepared state is noise-resilient, as evidenced by a clear interference pattern of the Wigner function in the presence of the sizable decoherence rate [Fig. 3a]. We also note that one can prepare mechanical Fock states of the membrane by employing a protocol proposed in Ref. [33].

The Rabi model and squeezed state.—The Hamiltonian \hat{H}_1 in Eq. (1) with a central qubit can be transformed into the Rabi Hamiltonian by setting $\delta_0 = 0$ and applying a spin rotation unitary transformation: $\hat{H}_R = (\Omega/2)\hat{\sigma}_z - g_0\hat{\sigma}_x(\hat{b} + \hat{b}^\dagger) + \omega_m\hat{b}^\dagger\hat{b}$. We emphasize that Ω is set by the microwave Rabi frequency, whose magnitude can be controlled independent of g_0 and ω_m and is only limited by the maximum input power that does not heat up the system. Therefore, a broad parameter regime of the Rabi model encompassing the ultrastrong and deep strong coupling regime [10–12], as shown in Fig. 2c, both in a resonant or dispersive limit can be explored here.

A particularly interesting achievable limit is $\Omega \gg g_0 \gg \omega_m$, in which finite-component systems of coupled spins and bosons, including the Rabi model, have been shown to undergo a superradiant phase transition [15, 16]. In the zeroth order in ω_m/Ω , one adiabatically eliminates the spin excited state to arrive at an effective Hamiltonian, $\hat{H}_{\text{eff}} = \omega_m\hat{b}^\dagger\hat{b} - (g_0^2/\Omega)(\hat{b} + \hat{b}^\dagger)^2 + \mathcal{O}(\omega_m/\Omega)$ [15]. For coupling strength $g_0 = \sqrt{\omega_m\Omega}/2$ the \hat{H}_{eff} becomes unstable marking the critical point of the Rabi model in the limit of $\omega_m/\Omega \rightarrow \infty$. For finite, but large Ω/ω_m , which can be realized in our setup, even though the higher order terms can no longer be neglected the short time dy-

namics is largely dominated by \hat{H}_{eff} . Noting that \hat{H}_{eff} includes the so-called single-mode squeezing terms, $\hat{b}^{\dagger 2}$ and \hat{b}^2 , we propose to use the strong microwave drive realizing the Rabi model to generate a squeezed state of the membrane: After the ground state cooling and the spin initialization, a resonant ($\delta_0 = 0$) microwave field with a Rabi frequency Ω is applied over a quarter of the mechanical period. By a projective readout of the qubit, a mechanical squeezed state will be prepared conditioned on the spin down outcome.

We simulate the protocol in the presence of decoherence and numerically calculate the variance of mechanical quadratures, $\hat{X}(\theta) \equiv \hat{b}e^{i\theta} + \hat{b}^\dagger e^{-i\theta}$, of the prepared states for a wide range of achievable values of ξ and Ω . The minimum variance values are presented in Fig. 3b in units of decibel. It shows a significant amount of squeezing, up to around -6.8 dB. The maximum squeezing is achieved for parameters close to the critical point $4g_0^2 = \omega_m\Omega$ (the blue line in Fig. 3b). The Wigner function of a final state clearly demonstrates that a squeezed state is indeed prepared. Note that we have used the master equation in the dressed basis in our numerical calculation [34].

Discussion.—Throughout the paper we have carried out simulations under the assumption that at each step only one of the qubits effectively manipulates the membrane and the other one remains idle. This indeed is justifiable because the cooling qubit is weakly coupled to the membrane and the magnetic field splitting $\Delta(r)$, and hence the detuning, for each qubit is different from one another which enables selective resonant driving [18].

For the spin qubit, possible intrinsic sources of decoherence include coupling of the spin to lattice vibrations, hyperfine interaction of the electron spin with the surrounding nuclear spins [35], noise in the external magnetic field [36], and spin dipole interaction with the other defects. The hyperfine effects are estimated to be negligible here as we assume splittings much larger than the hyperfine energies [37]. Moreover, the phonon DOS of hBN only exhibits large contributions at high frequencies [38]. At the low temperatures that we are considering here only the lowest vibrational modes can contribute in the decoherence with rate $\tilde{\Gamma}_v$. As an extrinsic source, the optical polarization process also leads to a qubit dephasing, that is comparable to the relaxation rate in size.

The proposed spin-mechanical setup offers the potential for a broad range of applications, which include ultrasensitive force detection [39, 40]. Also, the nonzero nuclear spins of nitrogen and boron stable isotopes give the opportunity of using the hBN flakes as a platform for quantum simulation of 2D spin systems, where the electronic spin of the color centers will realize their initialization, control, and readout [41].

Acknowledgements.—This work was supported by the Alexander von Humboldt foundation, the ERC Synergy grant BioQ, the EU STREP project EQUAM, the DFG CRC TRR21, and DFG FOR 1493. The authors also

acknowledge support by the state of Baden-Württemberg through bwHPC and the German Research Foundation (DFG) through grant no INST 40/467-1 FUGG.

-
- [1] T. T. Tran, K. Bray, M. J. Ford, M. Toth, and I. Aharonovich, *Nat. Nanotech.* **11**, 37 (2016).
 - [2] N. R. Jungwirth, B. Calderon, Y. Ji, M. G. Spencer, M. E. Flatté, and G. D. Fuchs, *Nano Lett.* **16**, 6052 (2016).
 - [3] N. Chejanovsky, M. Rezai, F. Paolucci, Y. Kim, T. Rendler, W. Rouabeh, F. F. de Oliveira, P. Herlinger, A. Denisenko, S. Yang, I. Gerhardt, A. Finkler, J. H. Smet, and J. Wrachtrup, *Nano Lett.* **16**, 7037 (2016).
 - [4] I. Aharonovich, D. Englund, and M. Toth, *Nat. Photon.* **10**, 631 (2016).
 - [5] C. Lee, Q. Li, W. Kalb, X.-Z. Liu, H. Berger, R. W. Carpick, and J. Hone, *Science* **328**, 76 (2010).
 - [6] L. Song, L. Ci, H. Lu, P. B. Sorokin, C. Jin, J. Ni, A. G. Kvashnin, D. G. Kvashnin, J. Lou, B. I. Yakobson, and P. M. Ajayan, *Nano Lett.* **10**, 3209 (2010).
 - [7] L. Boldrin, F. Scarpa, R. Chowdhury, and S. Adhikari, *Nanotechnology* **22**, 505702 (2011).
 - [8] C. Jin, F. Lin, K. Suenaga, and S. Iijima, *Phys. Rev. Lett.* **102**, 195505 (2009).
 - [9] C. Ciuti and I. Carusotto, *Phys. Rev. A* **74**, 033811 (2006).
 - [10] P. Forn-Díaz, J. Lisenfeld, D. Marcos, J. J. García-Ripoll, E. Solano, C. J. P. M. Harmans, and J. E. Mooij, *Phys. Rev. Lett.* **105**, 237001 (2010).
 - [11] T. Niemczyk, F. Deppe, H. Huebl, E. P. Menzel, F. Hocke, M. J. Schwarz, J. J. Garcia-Ripoll, D. Zueco, T. Hmmer, E. Solano, A. Marx, and R. Gross, *Nat. Phys.* **6**, 772 (2010).
 - [12] F. Yoshihara, T. Fuse, S. Ashhab, K. Kakuyanagi, S. Saito, and K. Semba, *Nat. Phys.* **13**, 44 (2016).
 - [13] A. D. Armour, M. P. Blencowe, and K. C. Schwab, *Phys. Rev. Lett.* **88**, 148301 (2002).
 - [14] M. Abdi, P. Degenfeld-Schonburg, M. Sameti, C. Navarrete-Benlloch, and M. J. Hartmann, *Phys. Rev. Lett.* **116**, 233604 (2016).
 - [15] M.-J. Hwang, R. Puebla, and M. B. Plenio, *Phys. Rev. Lett.* **115**, 180404 (2015).
 - [16] M.-J. Hwang and M. B. Plenio, *Phys. Rev. Lett.* **117**, 123602 (2016).
 - [17] R. Puebla, M.-J. Hwang, J. Casanova, and M. B. Plenio, *Phys. Rev. Lett.* **118**, 073001 (2017).
 - [18] See the supplementary information for more details on the group theory analysis of the defect, spin-polarization mechanism, and elasticity of the membrane.
 - [19] L. J. Rogers, K. D. Jahnke, M. H. Metsch, A. Sipahigil, J. M. Binder, T. Teraji, H. Sumiya, J. Isoya, M. D. Lukin, P. Hemmer, and F. Jelezko, *Phys. Rev. Lett.* **113**, 263602 (2014).
 - [20] L. Robledo, L. Childress, H. Bernien, B. Hensen, P. F. A. Alkemade, and R. Hanson, *Nature* **477**, 574 (2011).
 - [21] G. Grosso, H. Moon, B. Lienhard, S. Ali, D. K. Efetov, M. M. Furchi, P. Jarillo-Herrero, M. J. Ford, I. Aharonovich, and D. Englund, *arXiv:1611.03515 [cond-mat.mes-hall]* (2016).
 - [22] D. J. Wineland, C. Monroe, W. M. Itano, D. Leibfried, B. E. King, and D. M. Meekhof, *J. Res. Natl. Inst. Stand. Technol.* **103**, 259 (1998).
 - [23] H. J. Mamin, M. Poggio, C. L. Degen, and D. Rugar, *Nat. Nanotech.* **2**, 301 (2007).
 - [24] P. Rabl, P. Cappellaro, M. V. G. Dutt, L. Jiang, J. R. Maze, and M. D. Lukin, *Phys. Rev. B* **79**, 041302 (2009).
 - [25] M. S. Grinolds, M. Warner, K. D. Greve, Y. Dovzhenko, L. Thiel, R. L. Walsworth, S. Hong, P. Maletinsky, and A. Yacoby, *Nat. Nanotech.* **9**, 279 (2014).
 - [26] Y. Tao, A. Eichler, T. Holzherr, and C. Degen, *Nat. Commun.* **7**, 12714 (2016).
 - [27] I. Marzoli, J. I. Cirac, R. Blatt, and P. Zoller, *Phys. Rev. A* **49**, 2771 (1994).
 - [28] K. Jaehne, K. Hammerer, and M. Wallquist, *New J. Phys.* **10**, 095019 (2008).
 - [29] P. Rabl, *Phys. Rev. B* **82**, 165320 (2010).
 - [30] L. Tian, *Phys. Rev. B* **84**, 035417 (2011).
 - [31] B. Vlastakis, G. Kirchmair, Z. Leghtas, S. E. Nigg, L. Frunzio, S. M. Girvin, M. Mirrahimi, M. H. Devoret, and R. J. Schoelkopf, *Science* **342**, 607 (2013).
 - [32] W. H. Zurek, *Nature* **412**, 712 (2001).
 - [33] M. Abdi, M. Pernpeintner, R. Gross, H. Huebl, and M. J. Hartmann, *Phys. Rev. Lett.* **114**, 173602 (2015).
 - [34] F. Beaudoin, J. M. Gambetta, and A. Blais, *Phys. Rev. A* **84**, 043832 (2011).
 - [35] R. de Sousa and S. D. Sarma, *Phys. Rev. B* **68**, 115322 (2003).
 - [36] C. Roos, T. Zeiger, H. Rohde, H. C. Nägerl, J. Eschner, D. Leibfried, F. Schmidt-Kaler, and R. Blatt, *Phys. Rev. Lett.* **83**, 4713 (1999).
 - [37] I. Lovchinsky, J. D. Sanchez-Yamagishi, E. K. Urbach, S. Choi, S. Fang, T. I. Andersen, K. Watanabe, T. Taniguchi, A. Bylinskii, E. Kaxiras, P. Kim, H. Park, and M. D. Lukin, *Science* **355**, 503 (2017).
 - [38] J. Serrano, A. Bosak, R. Arenal, M. Krisch, K. Watanabe, T. Taniguchi, H. Kanda, A. Rubio, and L. Wirtz, *Phys. Rev. Lett.* **98**, 095503 (2007).
 - [39] J. Moser, J. Güttinger, A. Eichler, M. J. Esplandiu, D. E. Liu, M. I. Dykman, and A. Bachtold, *Nat. Nanotechnol.* **8**, 493 (2013).
 - [40] C. A. Muschik, S. Moulieras, A. Bachtold, F. H. L. Koppens, M. Lewenstein, and D. E. Chang, *Phys. Rev. Lett.* **112**, 223601 (2014).
 - [41] J. Cai, A. Retzker, F. Jelezko, and M. B. Plenio, *Nat. Phys.* **9**, 168 (2013).
 - [42] P. Giannozzi, S. Baroni, N. Bonini, M. Calandra, R. Car, C. Cavazzoni, D. Ceresoli, G. L. Chiarotti, M. Cococcioni, I. Dabo, A. D. Corso, S. de Gironcoli, S. Fabris, G. Fratesi, R. Gebauer, U. Gerstmann, C. Gougoussis, A. Kokalj, M. Lazzeri, L. Martin-Samos, N. Marzari, F. Mauri, R. Mazzarello, S. Paolini, A. Pasquarello, L. Paulatto, C. Sbraccia, S. Scandolo, G. Sclauzero, A. P. Seitsonen, A. Smogunov, P. Umari, and R. M. Wentzcovitch, *J. Phys.: Condens. Matter* **21**, 395502 (2009).
 - [43] C. M. Marian, “Reviews in computational chemistry,” (John Wiley & Sons, Inc., 2001) Chap. 3.
 - [44] T. T. Tran, C. Elbadawi, D. Totonjian, C. J. Lobo, G. Grosso, H. Moon, D. R. Englund, M. J. Ford, I. Aharonovich, and M. Toth, *ACS Nano* **10**, 7331 (2016).
 - [45] L. D. Landau and E. M. Lifshitz, *Theory of Elasticity* (Pergamon Press, 1975).

Supplemental Material: Spin-mechanics with color centers in hexagonal boron nitride membranes

MOLECULAR ORBITALS OF NEUTRAL $V_N N_B$

The geometry of the $V_N N_B$ defect is shown in Fig. S1b. It has a C_{2v} point group symmetry. The dangling-bonds are of sp^2 hybrid orbitals which are resulting from hybridization of $2s$ orbital with $2p_x$ and $2p_y$ orbitals and the $2p_z$ orbitals perpendicular to the plane. (The x -axis is the symmetry axis of the defect which goes from vacancy to the nitrogen atom and we have assumed the z -axis out of the plane of the material). We denote these dangling-bonds by $\{\sigma_N, \sigma_{B_1}, \sigma_{B_2}, \pi_N, \pi_{B_1}, \pi_{B_2}\}$ after the form of bonds they would create. That is, the σ refers to those which are in the plane (the sp^2 atomic orbitals) and π refers to the out of plane atomic orbitals. To facilitate the further analyses, one first finds the basis functions that diagonalize the Hamiltonian of the defect. In fact, this new basis turns out to be the ‘molecular orbitals’ (MOs). These MOs are linear combinations of the set of atomic orbitals, which represent the bases for the irreducible representations of the defect point group. For this reason, these linear combinations are called symmetry adapted linear combinations (SALCs):

$$a_1(1) = \alpha\sigma_N + \frac{\beta}{\sqrt{2}}(\sigma_{B_1} + \sigma_{B_2}), \quad (S1a)$$

$$a_1(2) = \beta\sigma_N + \frac{\alpha}{\sqrt{2}}(\sigma_{B_1} + \sigma_{B_2}), \quad (S1b)$$

$$b_1 = \frac{1}{\sqrt{2}}(\sigma_{B_1} - \sigma_{B_2}), \quad (S1c)$$

$$b_2(1) = \alpha'\pi_N + \frac{\beta'}{\sqrt{2}}(\pi_{B_1} + \pi_{B_2}), \quad (S1d)$$

$$b_2(2) = \beta'\pi_N + \frac{\alpha'}{\sqrt{2}}(\pi_{B_1} + \pi_{B_2}), \quad (S1e)$$

$$a_2 = \frac{1}{\sqrt{2}}(\pi_{B_1} - \pi_{B_2}), \quad (S1f)$$

where $|\alpha|^2 + |\beta|^2 = 1$ and $|\alpha'|^2 + |\beta'|^2 = 1$ and we have named the single-electron orbitals after the symmetry of the irreducible representation they transform. In a charge neutral defect each boron atom brings in one unpaired electron, while the nitrogen atom shares three electrons: two in its p_z orbital and one uncoupled in its sp^2 dangling-bond. In the ground state, these five electrons fill two orbitals and half-occupy the third. Our *ab initio* calculations show that the fully occupied $a_1(1)$ orbital resides deep in the valence band. Three of these orbitals with three occupant electrons are placed well-within the band-gap, which is consistent with previous results [1]. Meanwhile, two unoccupied orbitals are located in the conduction band. The explicit form of orbital wavefunctions suggest the electronic configuration sketched in Fig. S1. The energy spacing of the orbitals is such that the effect of those located in valence and conduction bands can be safely neglected. We thus only consider the band-gap orbitals and electrons in our study. Hence, the ground state is $[a_1]^2[b_2]^1[b'_2]^0$ and the first and second excited states are $[a_1]^1[b_2]^2[b'_2]^0$ and $[a_1]^2[b_2]^0[b'_2]^1$, respectively. Here, only the symmetry of orbitals are shown and the superscripts indicate the number of electrons occupying that orbital. And as a short hand we have taken b_2 for $b_2(1)$ and b'_2 for $b_2(2)$.

Since we have an odd number of electrons the state of the defect has a half-integer spin, thus, we need to work with the double group. The character table of \bar{C}_{2v} , the double group of C_{2v} , is shown in Table I. The ground and the excited states are both constructed by a filled singlet orbital and a half-occupied one. Therefore, their multi-electron spin state can only adopt antisymmetric doublet state. The total wavefunction of these electronic configurations in terms of Slater determinants are $|a_1\bar{a}_1\bar{b}_2\rangle$, $|a_1\bar{a}_1b_2\rangle$ for the ground state, $|\bar{a}_1b_2\bar{b}_2\rangle$, $|a_1b_2\bar{b}_2\rangle$ for the first excited state,

TABLE I. Character table of \bar{C}_{2v} point group. The double group is given, which is appropriate for the general case of odd number of electrons. The two rightmost columns show the functions which transform under a particular irreducible representation. Here, (x, y, z) stand for a polar vector, while (R_x, R_y, R_z) for an axial vector, like angular momenta.

\bar{C}_{2v}	E	\bar{E}	C_2, \bar{C}_2	$\sigma_v, \bar{\sigma}_v$	$\sigma'_v, \bar{\sigma}'_v$	functions	
A_1	1	1	1	1	1	x	x^2, y^2, z^2
A_2	1	1	1	-1	-1	R_x	yz
B_1	1	1	-1	1	-1	y, R_z	xy
B_2	1	1	-1	-1	1	z, R_y	xz
$E_{\frac{1}{2}}$	2	-2	0	0	0		

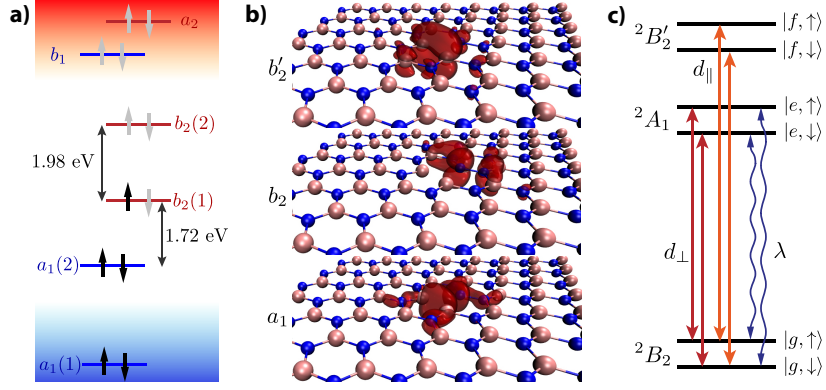


FIG. S1. a) Schematic band structure of hBN monolayer and position of the six defect molecular orbitals within it. Energy levels of the σ -type orbitals and π -type orbitals are distinguished by blue and red lines, respectively. Black and gray arrows indicate occupied and unoccupied states, respectively. b) Geometry of the $V_N N_B$ defect in hBN monolayer and the defect molecular orbitals who lay within the hBN band gap. c) Three lowest multi-electron states of the $V_N N_B$ defect and the respective dipole transitions and spin-orbit mixing.

and $|a_1 \bar{a}_1 \bar{b}_2\rangle$, $|a_1 \bar{a}_1 b'_2\rangle$ for the second excited state. Let us rename them to $\Psi = \{|g, \downarrow\rangle, |g, \uparrow\rangle, |e, \downarrow\rangle, |e, \uparrow\rangle, |f, \downarrow\rangle, |f, \uparrow\rangle\}$ in consistency with the main text notation.

AB INITIO COMPUTATIONS

In our *ab initio* computations, in order to have a well-isolated single $V_N N_B$ defect in a monolayer hBN membrane, we have used a super-cell with 8×8 hBN unit-cells and a layer of 15 Å vacuum on top of the sheet. Within the sheet, a nitrogen atom was removed (creating a vacancy), while one of its neighboring boron atoms was replaced by a nitrogen [see Fig. S1b or the schematics of Fig. 1a in the main text]. The structure was relaxed to its ground state using density-functional theory at local spin-density approximation and Perdew-Burke-Ernzerhof exchange-correlation functional level, with nonlinear core and scalar relativistic corrections. The two boron atoms and nitrogen at the vacancy were given an initial spin polarization. It was observed that when the two boron atoms of $V_N N_B$ defect have opposite spins, the system relaxes to its lowest energy level in agreement with the results of Ref. [1]. Consequently, the electronic band-structure and its density of states (DOS) of the $V_N N_B$ sheet was calculated. All the *ab initio* computations were carried out by Quantum-Espresso package [42], which is based on a plane-wave basis set and pseudo-potentials. The molecular orbitals shown in Fig. S1b have been built after a self-consistent calculation.

SPIN INTERACTIONS

We now study effect of the spin-orbit and spin-spin interactions on the properties of the defect by applying time-independent perturbation theory. Here, we assume that the crystal field is stronger than the spin interactions. This allows us to separate the orbital and spin parts of the total wavefunction, simplifying the calculations. As we will find out, the spin-orbit and spin-spin interactions do not lift the Kramers degeneracy of the states. However, they can mix the spin states of the electronic ground and excited states. In short notation, the spin-orbit interaction Hamiltonian is $H_{so} = \sum_j \sum_{\alpha} \ell_j^{\alpha} s_j^{\alpha}$, where $j = 1, 2, 3$ counts the number of particles, while α is for the irreducible representations of the orbital and spin angular momenta [43]. The group theory allows us to predict potentially nonzero matrix elements of a Hamiltonian. The quantity $\langle \psi | O | \phi \rangle$ vanishes if $\Gamma(\psi) \otimes \Gamma(O) \otimes \Gamma(\phi) \not\supset \Gamma_1$, where $\Gamma(\Xi)$ is the irreducible representation of Ξ and Γ_1 is the totally symmetric irreducible representation (for C_{2v} , $\Gamma_1 = A_1$). The spatial part of our wavefunctions transform either like A_1 or B_2 . Therefore, concerning the spatial parts, the non-vanishing elements can be summarized in the following tables:

$$\begin{array}{c|cc} O^{A_1} & A_1 & B_2 \\ \hline A_1 & \times & 0 \\ B_2 & 0 & \times \end{array}, \quad
 \begin{array}{c|cc} O^{A_2} & A_1 & B_2 \\ \hline A_1 & 0 & 0 \\ B_2 & 0 & 0 \end{array}, \quad
 \begin{array}{c|cc} O^{B_1} & A_1 & B_2 \\ \hline A_1 & 0 & 0 \\ B_2 & 0 & 0 \end{array}, \quad
 \begin{array}{c|cc} O^{B_2} & A_1 & B_2 \\ \hline A_1 & 0 & \times \\ B_2 & \times & 0 \end{array}$$

One thus concludes from the above tables that only the y component of the orbital angular momentum could give nonzero values. (The angular momenta transform like axial vectors and have no A_1 component). This simplifies the spin-orbit Hamiltonian into $H_{\text{so}} = \sum_j \ell_{y,j} s_{y,j}$.

The explicit form of spin-orbit Hamiltonian in the manifold of Ψ is:

$$H_{\text{so}} = \begin{pmatrix} 0 & 0 & 0 & \lambda & 0 & 0 \\ & 0 & \lambda & 0 & 0 & 0 \\ & & 0 & 0 & 0 & 0 \\ & & & 0 & 0 & 0 \\ & & & & 0 & 0 \\ & & & & & 0 \end{pmatrix}, \quad (\text{S2})$$

where we have introduced $\lambda = \frac{1}{2} \langle a_1 | \ell_y | b_2 \rangle$. While the $|f\rangle$ states remain unaffected, the first order correction to the ground and first excited eigenstates are

$$\widetilde{|g, \downarrow\rangle} = |g, \downarrow\rangle - \frac{\lambda}{\omega_0} |e, \uparrow\rangle, \quad (\text{S3a})$$

$$\widetilde{|g, \uparrow\rangle} = |g, \uparrow\rangle - \frac{\lambda}{\omega_0} |e, \downarrow\rangle, \quad (\text{S3b})$$

$$\widetilde{|e, \downarrow\rangle} = |e, \downarrow\rangle + \frac{\lambda^*}{\omega_0} |g, \uparrow\rangle, \quad (\text{S3c})$$

$$\widetilde{|e, \uparrow\rangle} = |e, \uparrow\rangle + \frac{\lambda^*}{\omega_0} |g, \downarrow\rangle, \quad (\text{S3d})$$

where $\hbar\omega_0 \approx 1.72$ eV is the energy difference between the ground and excited state. Another effect of spin is the direct magnetic dipole moment interaction between the species. We neglect the interaction of nuclear spin and the electronic spins, which introduce hyperfine structures to the system and only focus on such effects in the electronic system. Our analyses show that in the Ψ manifold the only effect of spin-spin interaction is inducing a shift in the energy levels, which does not lift the degeneracy.

SELECTION RULES

Now let us study the permitted optically induced transitions. Such transitions may happen via the dipole interaction: $H_{\text{di}} = \sum_j \sum_{\alpha} d_j^{\alpha} E_j^{\alpha}$, where $\mathbf{d} = e(x, y, z)$ is the dipole moment of the electron and \mathbf{E} is the electric field vector. Any polar vector (including the dipole moment) in C_{2v} transforms like (A_1, B_1, B_2) . The spin is just a spectator in this interaction. Hence, only the orbital symmetries and spin overlaps matter here. We remind that the x -axis is the symmetry axis of the defect connecting the vacancy to the nitrogen ion, which lies on the plane of the membrane. Generally, since the orbitals have either A_1 or B_2 symmetry, the allowed transitions are either induced by the axial component of the dipole moment $d_x \equiv d_{\parallel}$ (between orbitals with the same symmetry) or the out-of-plane component $d_z \equiv d_{\perp}$. In the zeroth-order, only d_{\perp} induced spin-preserving transitions are allowed. However, the spin-orbit mixing allows for d_{\parallel} -driven transitions associated with spin flip. For example, the dipole moments of $\widetilde{|g, \uparrow\rangle} \leftrightarrow \widetilde{|e, \downarrow\rangle}$ and $\widetilde{|g, \uparrow\rangle} \leftrightarrow \widetilde{|e, \uparrow\rangle}$ transitions are:

$$\langle \widetilde{g, \uparrow} | H_{\text{di}} | \widetilde{e, \downarrow} \rangle = \frac{\lambda}{\omega_0} (\langle a_1 | d_{\parallel} | a_1 \rangle + \langle b_2 | d_{\parallel} | b_2 \rangle) E_{\parallel} + \mathcal{O}(\frac{\lambda^2}{\omega_0^2}), \quad (\text{S4})$$

$$\langle \widetilde{g, \uparrow} | H_{\text{di}} | \widetilde{e, \uparrow} \rangle = \langle a_1 | d_{\perp} | b_2 \rangle E_{\perp} + \mathcal{O}(\frac{\lambda^2}{\omega_0^2}), \quad (\text{S5})$$

where we have used the fact that $\lambda^* = -\lambda$ concluded from anti-Hermitian nature of the angular momentum operators. This in principle, allows for optical spin polarization of the ground state.

We now conclude this part of the study by considering the energy diagrams in Fig. S1a and c and associating them with the experimental observations. For a 2D surface when irradiated by a perpendicular beam, the transition is more likely to happen via the in-plane dipole moments, which in our case is restricted to d_{\parallel} . That is, only x -polarized light will induce such transitions. Furthermore, transitions from first excited to the ground state induced by the axial moment d_{\parallel} are forbidden. So, d_{\parallel} only can make transitions between ground and the ‘second’ excited state. According to our *ab initio* calculations energy of photons emitted by such a transition is predicted to be about 1.98 eV. This is

indeed in agreement with the experimental observations and former *ab initio* studies on the polarization and frequency of the emitters [1–3, 44]. However, one notices that the non-axial dipole moment d_\perp , induced by out-of-plane electric polarization, may induce transitions from the first excited state to the ground state and result in emission of photons at 1.72 eV. One would naturally expect a higher brightness for the ‘axial’ emitters as the samples are irradiated perpendicularly.

MAGNETIC FIELD

An external magnetic field can alter dynamics of the system, either by shifting the energy levels or inducing interactions. The Zeeman Hamiltonian is given by $H_{Zee} = \mu_B \sum_j \sum_\alpha (\ell_j^\alpha + g_e s_j^\alpha) B^\alpha$, where μ_B is Bohr magneton, g_e is electron gyromagnetic ratio, and \mathbf{B} is the external magnetic induction. The orbital contribution in the energy shift of singlet orbitals is zero and only spin degeneracy of the energy levels are lifted according to their spin projection via the axial magnetic field component. The non-axial components of the field on the other hand can induce transitions between these spin-projection levels. For every spin doublet state manifold the Hamiltonian after a unitary transformation is

$$H_{Zee} = \frac{1}{2} \mu_B g_e \begin{pmatrix} +B_\perp & B_\parallel \\ B_\parallel^* & -B_\perp \end{pmatrix}. \quad (\text{S6})$$

The out-of-plane component thus produces the splitting $\Delta = \mu_B g_e B_\perp$, while the in-plane components when driven on resonance induce transitions between spin-up and spin-down states. To fulfill the resonance conditions the transitions only happen by oscillating magnetic fields at frequencies close to the splitting Δ . In our setup this is about GHz, the microwave pulses with in-plane polarizations thus can provide the required oscillating magnetic field.

SPIN POLARIZATION

One exploits the 2D nature of the hexagonal boron nitride mono-layers to enhance the weak spin-flip transitions over the allowed spin preserving transitions. Assume the system is initially prepared in state $\widetilde{|g, \uparrow\rangle}$. For an exciting laser at frequency $\omega_L = \omega_0 - \Delta$ the rates at which the excited states $\widetilde{|e, \downarrow\rangle}$ and $\widetilde{|e, \uparrow\rangle}$ get populated are given by

$$R_{23} = \frac{|\mathcal{E}_\parallel|^2}{2\kappa}, \quad (\text{S7})$$

$$R_{24} = \frac{|\mathcal{E}_\perp|^2 \kappa}{2(\kappa^2 + \Delta^2)}, \quad (\text{S8})$$

where $\mathcal{E}_\parallel = (\lambda/\omega_0)(\langle a_1 | d_\parallel | a_1 \rangle + \langle b_2 | d_\parallel | b_2 \rangle) E_\parallel$ and $\mathcal{E}_\perp = \langle a_1 | d_\perp | b_2 \rangle E_\perp$ are the in-plane and out-of-plane semiclassical Rabi frequencies, respectively. The ratio is hence

$$\frac{R_{24}}{R_{23}} = \left| \frac{\mathcal{E}_\perp}{\mathcal{E}_\parallel} \right|^2 \frac{\kappa^2}{\kappa^2 + \Delta^2}. \quad (\text{S9})$$

For well-collimated light perpendicularly shining on the surface of the membrane, the in-plane component of the electric field is much larger than its out-of-plane component $E_\perp \ll E_\parallel$. The dipole moments ratio on the other hand is dominantly determined by the factor $\lambda/\omega_0 \ll 1$. In practice one needs to achieve $\lambda/\omega_0 \sim E_\parallel/E_\perp$, therefore, the population ratio will be dominantly determined by κ/Δ , which in turn could be made quite small. Therefore, the system ends-up in $\widetilde{|g, \downarrow\rangle}$. Similarly, an optical excitation at frequency $\omega_L = \omega_0 + \Delta$ can eventually bring the system to $\widetilde{|g, \uparrow\rangle}$.

ELASTICITY OF THE MEMBRANE

In this section we present the mechanical model we have taken for describing the motion of the membrane. Let us denote the vertical displacement of the membrane by $\zeta(x, y)$ with respect to its resting plane. Its equation of motion is [45],

$$\rho h \partial_t^2 \zeta = -D \nabla^2 \nabla^2 \zeta + T \nabla^2 \zeta, \quad (\text{S10})$$

where ∇^2 is the two-dimensional (2D) Laplacian, ρ is the mass density, and $D = Yh^3/[12(1 - \sigma^2)]$ with Y being the Young modulus, h the thickness of the membrane, and σ its Poisson ratio. Here, $T = T_0 + \Delta T$ is the total tensile force experienced by the membrane. T_0 is the force applied by the support and ΔT is the bending tension. The latter is proportional to the relative change in the surface area of the membrane. For a circular membrane of radius R it is given by

$$\Delta T = Yh \frac{\Delta A}{A_0} = \frac{Yh}{2A_0} \int_0^{2\pi} d\theta \int_0^R r dr |\nabla \zeta|^2. \quad (\text{S11})$$

Here, A_0 is the the area at rest. Typically, for membranes the bending tension is much smaller than the tensile force on the edges of the membrane ($D\nabla^2\nabla^2\zeta \ll T_0\nabla^2\zeta$). Thus the equation (S10) is simplified to

$$\rho h \partial_t^2 \zeta = T_0 \nabla^2 \zeta, \quad (\text{S12})$$

where we have neglected the nonlinear terms assuming small oscillation amplitudes.

By applying the method of separation of variables $\zeta(r, \theta, t) = \sum_{n=0}^{\infty} X_n(t) \psi_n(r, \theta)$ the normal-modes are found to be $\psi_n(r, \theta) = \mathcal{A}_n J_{k_n}(\lambda_n r/R) \cos k_n \theta$, where J_k are Bessel functions of the first kind, $k_n \in \mathbb{Z}$. Here, λ_n are the zeros of Bessel functions [14]. We choose \mathcal{A}_n such that $\max\{\psi_n\} = 1$ so that X_n provides the maximal vertical deflection of the membrane when the corresponding mode is excited. Dynamics of each mode is obtained by inserting $\zeta(r, \theta, t)$ into Eq. (S12), multiplying both sides of the resulting equation by $\psi_m(r, \theta)$, and integrating over the surface of the membrane. This leads to

$$m_n^* \ddot{X}_n + \mathcal{K}_n X_n = 0. \quad (\text{S13})$$

Here $m_n^* = \mu_{2D} \int_0^{2\pi} d\theta \int_0^R r dr \psi_n^2$ is the effective mass and $\mathcal{K}_n = T_0 \int_0^{2\pi} d\theta \int_0^R r dr |\nabla \psi_n|^2$ the mode's spring constant. Therefore, the dynamics of the membrane can be described by the Hamiltonian

$$H_m = \sum_{n=0}^{\infty} \left(\frac{P_n^2}{2m_n^*} + \frac{1}{2} m_n^* \omega_{m,n}^2 X_n^2 \right), \quad (\text{S14})$$

where we have defined mode frequency $\omega_{m,n} = \sqrt{\mathcal{K}_n/m_n^*}$. For the fundamental mode $n = 0$, which we have taken as our mechanical mode in the main text, we obtain the following expressions for the Hamiltonian parameters in terms of physical parameters:

$$m_0^* \approx 0.27 \times (\pi R^2) \rho h, \quad (\text{S15a})$$

$$\omega_{m,0} \approx 2.4 \times \sqrt{\frac{T_0}{\rho h R^2}}. \quad (\text{S15b})$$

These relations are used throughout the paper for computing the mechanical mode frequency $\omega_m \equiv \omega_{m,0}$ and mass $m \equiv m_0^*$ —appearing in the zero-point motion amplitude and hence the spin-motion coupling rate.

EFFECT OF THE CENTER QUBIT ON COOLING

Throughout the paper we have assumed that at each step only one of the qubits couples to the membrane and the other one remains idle. Here, we show that this indeed is the case and those ‘unwanted’ couplings do not affect functioning of the ‘wanted’ ones. The crucial case may happen in the cooling process, where the large coupling of the central qubit may hinder ground state cooling. Let us first write down the full Hamiltonian:

$$\begin{aligned} \hat{H}_2 = & -\frac{\delta_0}{2} \hat{\sigma}_{z,0} - \frac{\delta_c}{2} \hat{\sigma}_{z,c} + \frac{\Omega}{2} (\hat{\sigma}_{x,0} + \hat{\sigma}_{x,c}) \\ & + (g_0 \hat{\sigma}_{z,0} + g_c \hat{\sigma}_{z,c}) (\hat{b} + \hat{b}^\dagger) + \omega_m \hat{b}^\dagger \hat{b}. \end{aligned} \quad (\text{S16})$$

Here, we have taken one microwave drive, and therefore, the same Rabi frequencies, even though the central Rabi frequency could be smaller for two other possible orientations of $V_N N_B$ defect. For cooling, the optimal microwave

drive parameters are $\omega_D \approx \Delta_c - \omega_m$ and $\Omega < \omega_m$, where Δ_c is the magnetic splitting of the cooling qubit. This brings Eq. (S16) to

$$\begin{aligned} \hat{H}_2 \approx & \frac{\omega_m}{2} \hat{\sigma}_{z,c} + \frac{\Omega}{2} \hat{\sigma}_{x,c} + g_c \hat{\sigma}_{z,c} (\hat{b} + \hat{b}^\dagger) \\ & + \left(\frac{\Delta_0 - \Delta_c}{2} + g_0 (\hat{b} + \hat{b}^\dagger) \right) \hat{\sigma}_{z,0} + \omega_m \hat{b}^\dagger \hat{b}, \end{aligned} \quad (\text{S17})$$

where $\Delta_0 = \Delta(0)$ is the magnetic field splitting of the central qubit and $|\Delta_0 - \Delta_c| \gg \omega_m$ is employed in the approximations. Since the central qubit is not externally driven, it will mostly stay in its ground state due to the optical relaxation. Therefore, sole effect of the second line in Eq. (S17) is a shift in the total energy of the system and position quadrature of the mechanical mode. That is, the system will end up in a displaced thermal state. We have proven this by numerically solving the master equation with Hamiltonian (S17) and a generalized version of the Liouvillian Eq. (2) in the main text. It is noteworthy that since in this working regime the system composed of the central qubit and the mechanical mode is already diagonalized, the independent dissipators are valid. The resulting states are coherent thermal states with thermal phonon numbers reported in Fig. 3c of the main text.

During state preparation protocol the microwave rotation pulses are targeting the central qubit and thus $\omega_D \approx \Delta_0$. Therefore, the cooling qubit is essentially off-resonance as $\Delta_c < \Delta_0$. (For example, when $R = 1 \mu\text{m}$ one gets $\Delta_c \approx 0.4\Delta_0$ and for $R = 3 \mu\text{m}$ it is $\Delta_c \approx 0.2\Delta_0$). Adding to this, weak coupling character of the cooling qubit $g_c \lesssim \omega_m$, its effect on the dynamics becomes negligible. The same story applies for the Rabi superradiance phase transition process.